Stanford Exploration Project, Report 115, May 22, 2004, pages 71–81

Short Note

Surface boundary condition for one-way wave equation shot-profile migration

Alejandro A. Valenciano, Thomas Tisserant, and Biondo Biondi[1]

INTRODUCTION

The one-way approximation to the full wave equation has been widely used for imaging the earth's interior (Claerbout, 1985). This approximation ignores back-scattering in the wavefield but usually works well with surface seismic data. In the shot-profile migration scheme, two one-way wave equations need to be solved. One downward extrapolates the source wavefield and the other downward extrapolates the receiver wavefield. By using an imaging condition, the subsurface image is formed (Claerbout, 1971).

Usually, the initial surface boundary condition for downward extrapolating the source wavefield is chosen to be an impulse convolved with a wavelet at the shot position. However, downward extrapolation with the one-way wave equation requires boundary conditions on the surface, $z = 0$, at all locations and all times. Since horizontal (or high-propagation-angle) waves, reflected waves, and overturned waves can all contribute to the surface wavefield, it appears that the full solution must already be known in order to supply these initial data (Nichols, 1994).

Zhang (1993) proposes two correction terms to the traditional one-way wave equations. One is a correction for the source and receiver wavefields extrapolation, while the other is a new boundary condition for the source wavefield. This new boundary condition is not only an impulse at the shot position but also includes contributions at different times and surface positions, depending on the surface velocity.

In this short note, we introduce an alternative surface boundary condition for the source wavefield downward extrapolation i.e, the Green function corresponding to the Helmholtz equation for a constant velocity medium at $z = 0$. It includes contributions at different times and surface positions depending on the surface velocity, similar to Zhang's boundary condition, but differs in the amplitude.

We compare the wavefront amplitudes calculated using the new surface boundary condition, the traditional surface boundary condition, and Zhang's surface boundary condition. The

[1]**email:** valenciano@sep.stanford.edu, thomas@sep.stanford.edu, biondo@sep.stanford.edu

comparisons are made using three synthetic velocity models: constant, vertically varying, and Marmousi. The results show that the new surface boundary condition produces more balanced wavefronts in the constant-velocity model and in the vertically varying velocity model (VOZ) and behaves similarly to Zhang's in the Marmousi velocity model.

SURFACE BOUNDARY CONDITIONS

Point source

The traditional boundary condition for the source wavefield extrapolation with the one-way wave equation (Claerbout, 1985) can be written as follows:

$$D(\mathbf{x}, z=0;\omega) = W(\omega)\delta(\mathbf{x}-\mathbf{x}_s), \tag{1}$$

where $D(\mathbf{x}, z=0;\omega)$ is the source wavefield at the surface, $W(\omega)$ is the wavelet, and $\delta(\mathbf{x}-\mathbf{x}_s)$ is an impulse at the shot position $\mathbf{x}_s$. Although kinematically correct, Claerbout's scheme fails to provide the correct wavefield amplitudes.

WKBJ approximation

Zhang (1993) proposes a different surface boundary condition, together with a correction for the source and receiver wavefields extrapolation, aiming to improve the dynamic information of the one-way wave equation. Zhang et al. (2001) apply this surface boundary condition to obtain a true-amplitude shot profile migration result in the WKBJ sense (Shan and Biondi, 2003). Zhang's surface boundary condition is stated as follows:

$$p_D(\mathbf{x}, z=0;\omega) \;=\; \frac{1}{2}\Lambda^{-1} W(\omega)\delta(\mathbf{x}-\mathbf{x}_s), \tag{2}$$

where

$$\Lambda \;=\; ik_z = i\sqrt{\frac{\omega^2}{v^2} - \mathbf{k}^2}, \tag{3}$$

$p_D(\mathbf{x}, z=0;\omega)$ is the new source wavefield that satisfies the corrected one-way wave equation (Zhang et al., 2001), Λ is the square-root operator, v is the medium velocity, k_z is the vertical wavenumber, and $\mathbf{k} = (k_x, k_y)$ is the horizontal wavenumber vector.

This boundary condition is not only an impulse at the shot position (Figure 1a) but also includes a contribution at different times and surface positions depending on the surface velocity (Figure 1b). This appears to resolve the contradiction discussed by Nichols (1994), by creating a V-shaped curve as the surface boundary condition. It mimics a wavefield with a high angle of propagation at the surface, resulting in more homogeneous wavefronts.

The implementation of Zhang's surface boundary condition has the disadvantage that the square root operator (Λ) is undefined for high values of the spatial wavenumber. That is why there is the need of establishing a cut off for the spatial wavenumber limiting the accuracy of the steep angles.

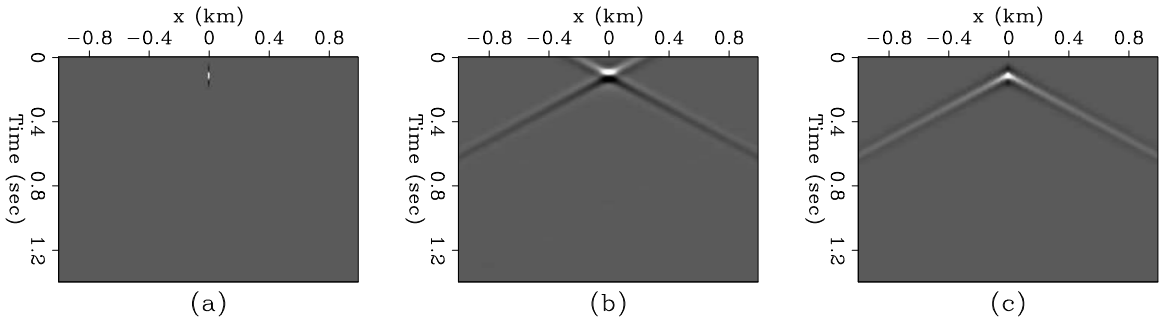

Figure 1: Surface boundary condition (a) traditional, (b) Zhang's, and (c) Green function. alejandro2-comp_v [CR]

Green function of the Helmholtz equation

Another possible surface boundary condition could be the Green function of the Helmholtz equation for a constant velocity medium at $z = 0$, convolved with the wavelet:

$$D_g(\mathbf{x}, z = 0; \omega) = W(\omega) G(\mathbf{x}, z = 0; \omega), \tag{4}$$

where

$$G(\mathbf{x}, z = 0; \omega) = \frac{1}{4\pi r} e^{i \frac{\omega r}{v}}, \tag{5}$$

is the Green function at the surface, $W(\omega)$ is the wavelet, and r is the distance to the shot position.

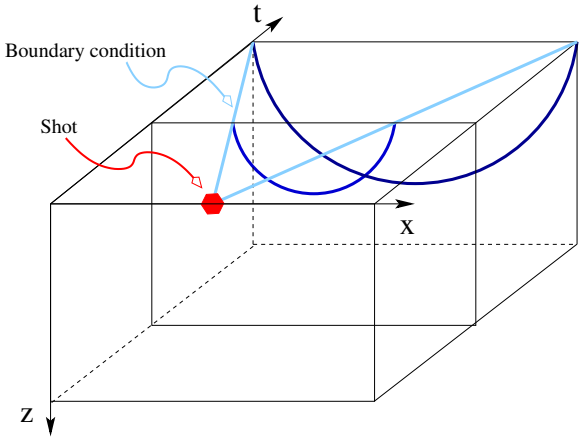

Figure 2: Surface boundary condition for the source wavefield. alejandro2-cube_bc [NR]

The idea is illustrated in Figure 2, where a linear moveout depending on the surface velocity dictates the time-position of the wavefront. As time increases, the amplitude should decay as the inverse of the distance to the shot position (geometrical spreading). Figure 1c shows the new boundary condition.

As oppose to Zhang's approximation the Green function is computed without the need of the square root operator. Thus, there is no need of cutting off the spatial wavenumbers. This allows to keep the accuracy of the steep angles.

RESULTS

Constant velocity medium

Figure 3 shows a comparison of three snapshots in the (x,z) plane of the source wavefield computed for the three different surface boundary conditions in a constant-velocity medium, with phase-shift extrapolation. Ideally the wavefront amplitude should be homogeneous with propagation angle.

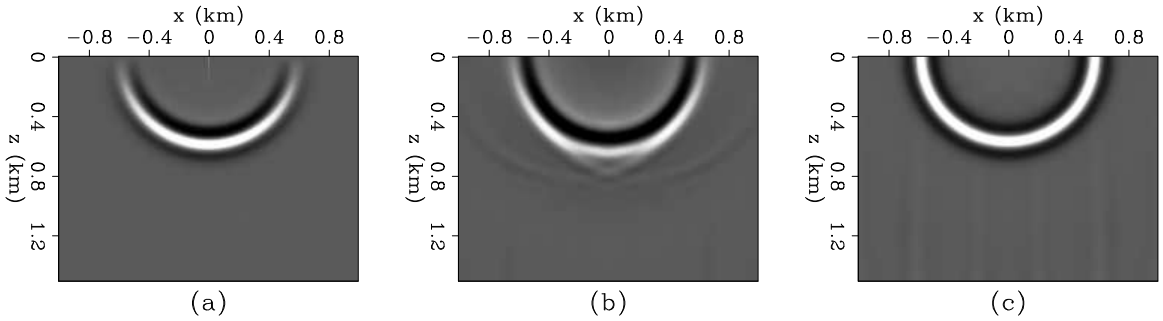

Figure 3: Snapshot of the source wavefield in a constant velocity medium using (a) the traditional surface boundary condition, (b) Zhang's surface boundary condition, and (c) the new surface boundary condition. alejandro2-comp_wfld [CR]

Figure 4 shows a comparison of the amplitudes along the wavefront depending on the propagation angle. We can see that for the traditional surface boundary condition (dotted curve), the amplitude along the wavefront is not uniform–it is high for sub-vertical propagation, but it fades away at higher angles and completely disappears for horizontal propagation. The curve corresponding to Zhang's surface boundary condition (dashed curve), although behaving better than the traditional one, fails to produce the correct amplitude at high propagation angles. On the other hand, the proposed surface boundary condition (solid curve) presents homogeneous amplitude at every angle.

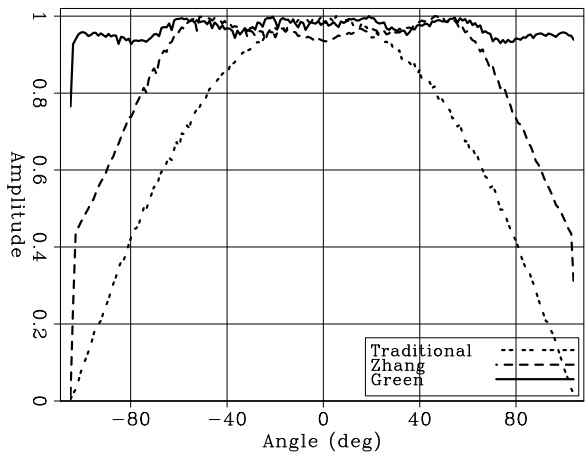

Figure 4: Amplitudes along the wavefields in a constant velocity medium. alejandro2-comp_max [CR]

Vertically varying velocity (VOZ) medium

Figure 5 shows a comparison of three snapshots in the (x,z) plane of the source wavefield computed for the three different surface boundary conditions in a VOZ medium. The extrapolation method used was phase-shift.

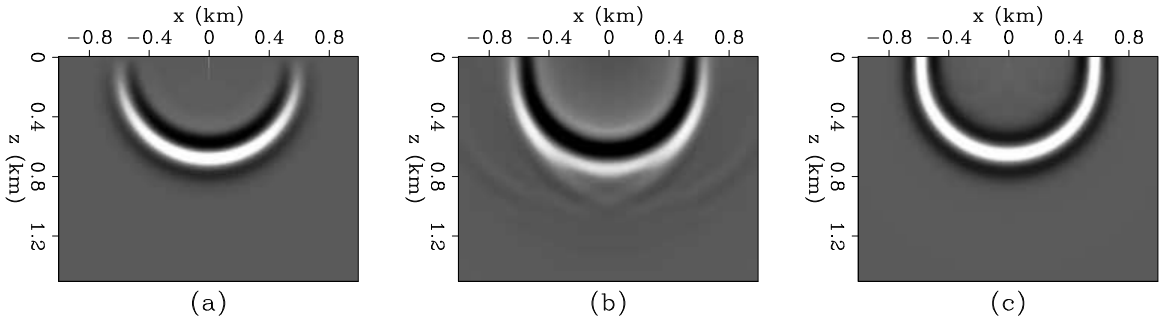

Figure 5: Snapshot of the source wavefield in a vertically varying velocity using (a) the traditional surface boundary condition (b) Zhang's surface boundary condition (c) the new surface boundary condition. alejandro2-comp_wfld_voz [CR]

Figure 6 shows a comparison of the amplitudes along the wavefront depending on the propagation angle. We can see that for the traditional surface boundary condition (dotted curve), the amplitude along the wavefront fails to follow the theoretical trend (Winbow, 1995) (dot-dash curve)–it is high for sub-vertical propagation, but it fades away at higher angle and completely disappears for horizontal propagation. The curve corresponding to Zhang's surface boundary condition (dashed curve) and the curve corresponding to the proposed surface boundary condition (solid curve) match the theoretical curve up to 70°. After that angle, Zhang's surface boundary condition gives a lower value than the theoretical while the proposed surface boundary condition gives a higher value than the theoretical. Overall, the curve corresponding to the proposed surface boundary condition agrees better with the theoretical curve.

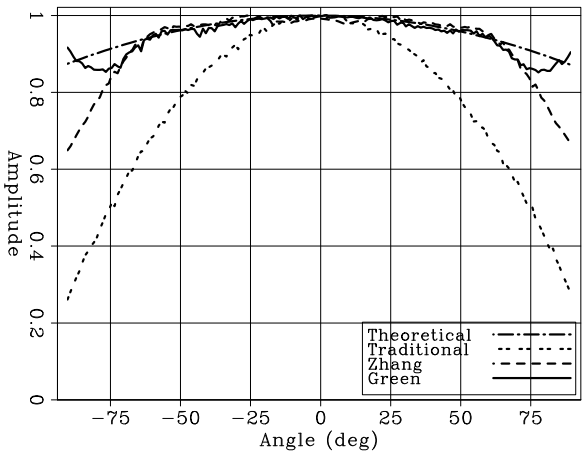

Figure 6: Amplitudes along the wavefields in a voz medium. alejandro2-comp_max_voz_Dickens_bis [CR]

Complex velocity medium (Marmousi)

The Marmousi synthetic data set (Bourgeois et al., 1991) was first released as a blind test for velocity estimation. It has become a popular testbed for migration algorithms. Its structural style is dominated by growth faults, which arise from salt creep and give rise to the complicated velocity structure in the upper part of the model.

Figure 7 shows a comparison of three snapshots in the (x,z) plane of the source wavefield, computed using the three different surface boundary conditions in the Marmousi model. The extrapolation method used was split-step with 7 reference velocities (Stoffa et al., 1990). In the Marmousi model, the wavefront amplitude should not be homogeneous with the propagation angle. This is because of the complexity of the velocity model.

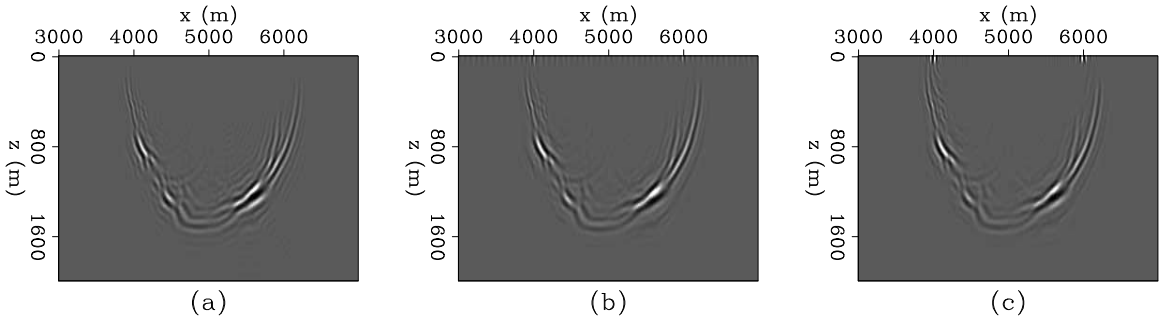

Figure 7: Snapshot of the source wavefield in the Marmousi velocity model using (a) the traditional surface boundary condition, (b) Zhang's surface boundary condition, and (c) the new surface boundary condition. alejandro2-comp_wfld_Marm [CR]

Figure 8 shows a comparison of the amplitudes along the wavefront depending on the polar angle (polar system center at the shot position). We can see that the amplitudes along the wavefront have a complex behavior. In general, for the traditional surface boundary condition (dotted curve), the wavefront shows lower amplitudes at higher angles than do the curves corresponding to Zhang's surface boundary condition (dashed curve) and the proposed surface boundary condition (solid curve).

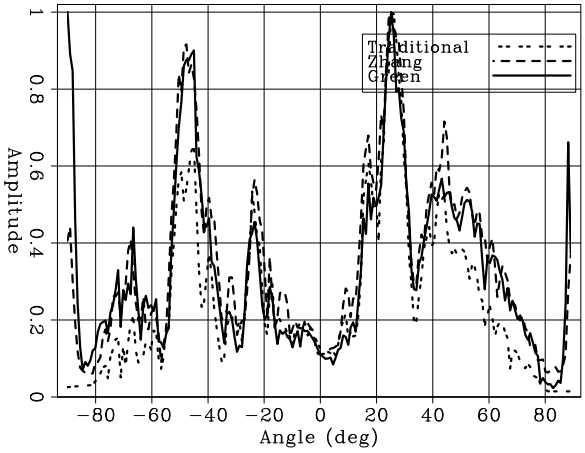

Figure 8: Amplitudes along the wavefields in the Marmousi velocity model. alejandro2-comp_max_Marm [CR]

We migrated the Marmousi model data with a split-step algorithm using 7 reference velocities. Figures 9a and 10a show the image obtained using the traditional surface boundary condition, figures 9b and 10b show the image obtained using Zhang's surface boundary condition, and figures 9c and 10c show the image obtained using the new surface boundary condition. Both figure 9b (10b) and figure 9c (10c) show steep dips more accurately than 9a (10a).

CONCLUSIONS

We presented a new surface boundary condition for downward continuation using the one-way wave equation which improves the amplitude distribution along the wavefronts. This new surface boundary condition is the Green function of the Helmholtz equation for a constant velocity medium at $z = 0$. The results, in both the constant velocity and VOZ models, show that the new surface boundary condition produces wavefront amplitudes that match better the theoretical curve than the traditional and Zhang's.

Both Zhang's surface boundary condition and the Green function surface boundary condition behave similarly in the Marmousi velocity model, resulting in better imaging of steep dips than those obtained with the traditional surface boundary condition.

More research needs to be done to study the AVA amplitude responses and phase differences due to the use of different surface boundary conditions.

ACKNOWLEDGMENT

We thank Tom Dickens for pointing to a reference for the theoretical Green function in the 2D VOZ medium and for important suggestions. We also thank Anatoly Baumstein and John Anderson for insightful discussions.

REFERENCES

Bourgeois, A., Bourget, M., Lailly, P., Poulet, M., Ricarte, P., and Versteeg, R., 1991, Marmousi, model and data: Eur. Assoc. Expl. Geophys., in Versteeg, R., and Grau, G., Eds., The Marmousi experience, Proceedings of the 1990 EAEG workshop on Practical Aspects of Seismic Data Inversion, 5–16.

Claerbout, J. F., 1971, Toward a unified theory of reflector mapping: Geophysics, **36**, no. 3, 467–481.

Claerbout, J. F., 1985, Imaging the Earth's Interior: Blackwell Scientific Publications.

Nichols, D. E., 1994, Imaging complex structures using band-limited Green's functions: SEP–**81**.

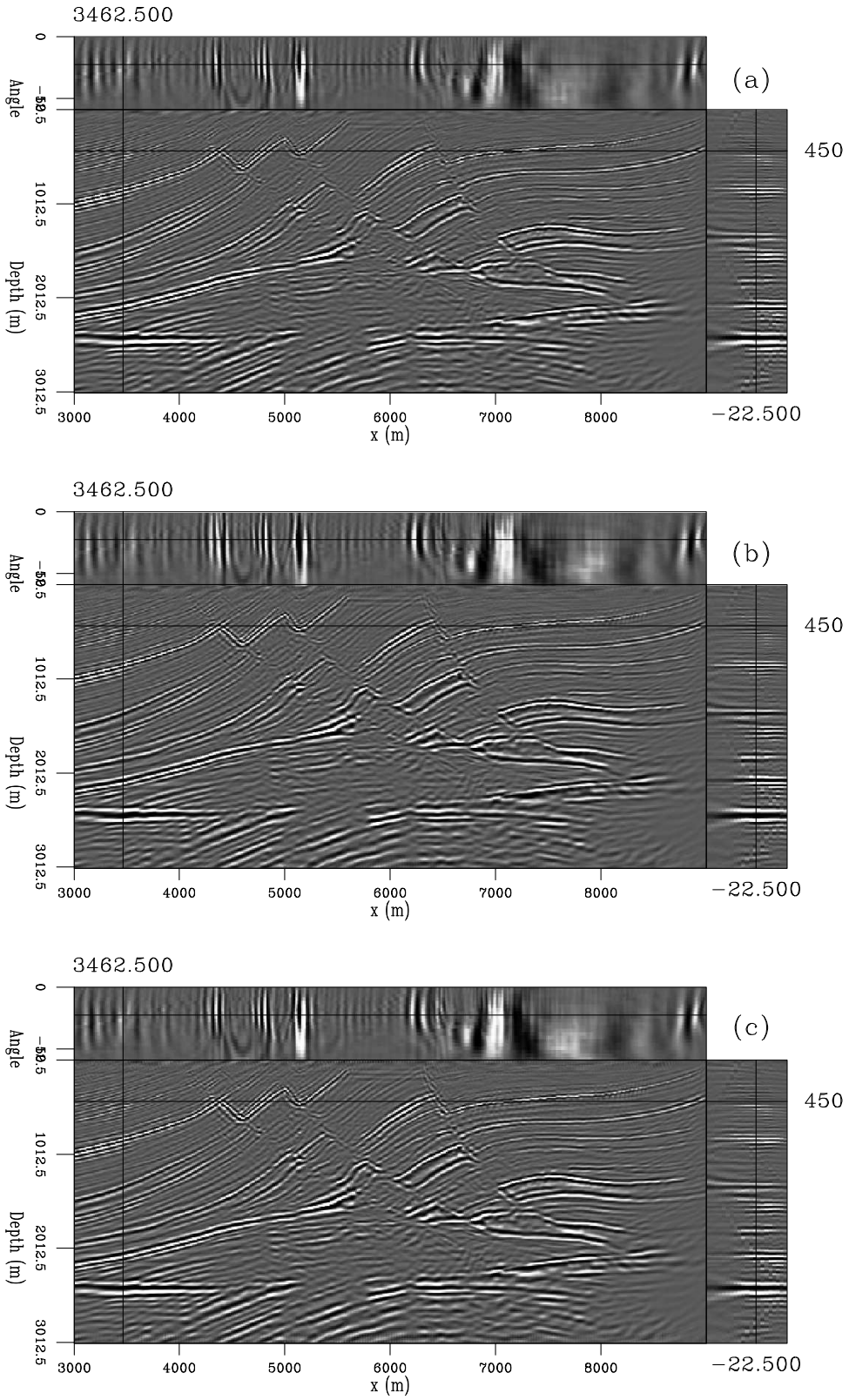

Figure 9: Marmousi image using (a) the traditional surface boundary condition, (b) Zhang's surface boundary condition, and (c) the new surface boundary condition. alejandro2-imag_ang [CR]

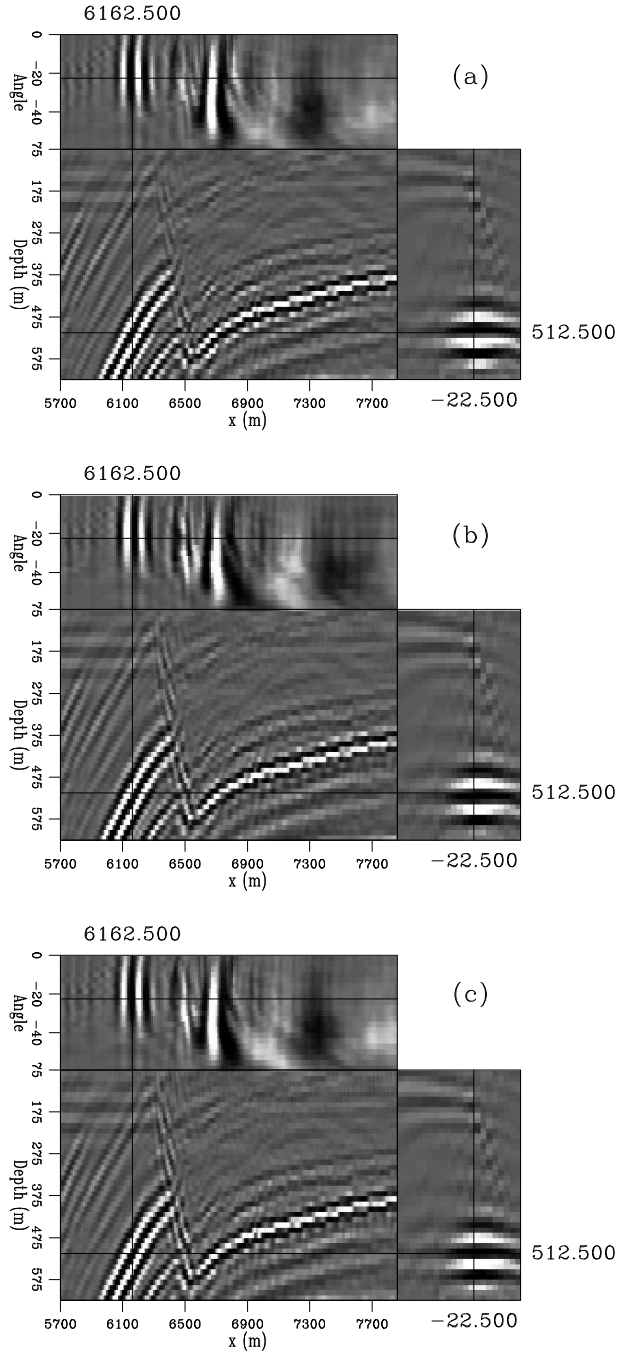

Figure 10: Close-up of the Marmousi image using (a) the traditional surface boundary condition, (b) Zhang's surface boundary condition, and (c) the new surface boundary condition. alejandro2-imag_ang_zoom [CR]

Shan, G., and Biondi, B., 2003, WKBJ and amplitude preserving one-way wave equation: SEP–**114**, 67–70.

Stoffa, P. L., Fokkema, J. T., de Luna Freire, R. M., and Kessinger, W. P., 1990, Split-step Fourier migration: Geophysics, **55**, no. 4, 410–421.

Winbow, G. A., 1995, Controlled amplitude time migration: Soc. of Expl. Geophys., 65th Ann. Internat. Mtg, 1153–1155.

Zhang, Y., Sun, J., Notfors, C., Bleistein, N., and Zhang, G., 2001, Towards accurate amplitudes for one-way wavefield extrapolation of 3-D common shot records: 71st Ann. Internat. Mtg., Soc. of Expl. Geophys., Workshop presentation.

Zhang, G., 1993, System of coupled equations for upgoing and downgoing waves: Acta Math. Appl. Sinica, **16**, no. 2, 251–263.